npj Science of Food

https://doi.org/10.1038/s41538-026-00874-9

Article in Press

Novel insights into the binding mechanisms of selected aldehydes during heat-induced protein unfolding

Received: 25 December 2025

Accepted: 28 April 2026

Cite this article as: Wang, J., Wang, T., Yang, P. *et al.* Novel insights into the binding mechanisms of selected aldehydes during heat-induced protein unfolding. *npj Sci Food* (2026). https://doi.org/10.1038/s41538-026-00874-9

Jingfan Wang, Tianze Wang, Ping Yang, Dong Han, Chunhui Zhang, Wei Jia, Giorgia Purcaro & Marie-Laure Fauconnier

Novel insights into the binding mechanisms of selected aldehydes during heat-induced protein unfolding

Jingfan Wang [a,b,c,1], Tianze Wang [a,1], Ping Yang [a], Dong Han [a]*, Chunhui Zhang [a]*, Wei Jia, Giorgia Purcaro[c], Marie-Laure Fauconnier[b]

a Key Laboratory of Agro-Products Processing, Ministry of Agriculture and Rural Affairs, Institute of Food Science and Technology, Chinese Academy of Agricultural Sciences, Beijing 100193, China

b Laboratory of Chemistry of Natural Molecules, Gembloux Agro-Bio Tech, University of Liege, 5030 Gembloux, Belgium

c Laboratory of Analytical Chemistry, Gembloux Agro-Bio Tech, University of Liège, 030, Gembloux, Belgium

*Corresponding author: contributes equally

To whom correspondence should be addressed: dr_zch@163.com (Zhang, C); orange_1101@126.com (Han, D)

1 The authors contributed equally to this article

Abstract

This investigation aimed to clarify the binding mechanisms between six aldehydes and myofibrillar proteins (MPs), with a structural explanation in response to stage-heating treatments. The conformational intermediates of MPs, which form during heat processing, were systematically characterized to elucidate their role in aldehyde binding and flavor retention. Machine learning results suggested that high-temperature boiling promoted extensive protein denaturation and aggregation, while subsequent low-temperature stewing induced partial rearrangement. Thermodynamic parameters indicated that hexanal–MPs formation was primarily driven by hydrogen bonding, whereas other longer-chain and unsaturated aldehydes penetrated hydrophobic pockets. Proteomics revealed that saturated aldehydes predominantly formed Schiff bases with the lysine ε-amino group. Unsaturated aldehydes, especially (*E, E*)-2,4-decadienal, undergo both Schiff base reactions and Michael addition with cysteine, histidine, and tryptophan residues. The retention/release behavior of aldehydes during processing is determined by covalent and non-covalent interactions. These results provide a scientific basis for precisely controlling flavor quality in meat products.

KEYWORDS: beef protein, aldehydes, covalent interaction, stage-thermal treatment, proteomics.

1. Introduction

Stewed beef with spices (SBS) is a popular traditional meat product characterized by its distinctive aroma. The perception of characteristic aromas in cooked meat products is determined by the binding between myofibrillar proteins (MPs) and aroma compounds (ACs). The unique flavor of SBS is developed through a variety of complicated thermal reactions, including the Maillard reaction, lipid oxidation, and spice infusion, during the stewing and

soaking processes[1]. Among the volatile compounds identified in SBS, aliphatic aldehyde compounds (ACs) like hexanal, octanal, nonanal, (*E*)-2-undecenal, and (*E, E*)-2,4-decadienal are recognized as major contributors to the characteristic aroma[1]. Besides, the relatively simple molecular structures and reactive carbonyl groups make aldehydes possible to elucidate both covalent and non-covalent binding mechanisms. These aldehydes are primarily generated from the oxidation and degradation of polyunsaturated fatty acids, such as linoleic and arachidonic acids[2]. Hexanal, a saturated C6 aldehyde, imparts green and grassy aroma. Octanal and nonanal, which are medium-chain saturated aldehydes (C8–C9), contribute citrus and fatty nuances that enhance the overall richness of the meat flavor [3]. In contrast, (*E*)-2-decenal, (*E*)-2-undecenal, and, in particular, (*E, E*)-2,4-decadienal are classified as α, β-unsaturated and polyunsaturated aldehydes with highly electrophilic properties. These longer-chain unsaturated aldehydes are responsible for fatty aroma, which plays a crucial role in the intensity of aroma perceived by consumers. Their presence is highly sensitive to heating temperature and time. Aldehydes are major secondary lipid oxidation products formed via β-scission of lipid hydroperoxides, and they play a central role in determining both flavor quality and oxidative stability in meat products. Despite their importance, the release and retention behaviors of these structurally diverse ACs in real processing conditions have yet to be clarified.

The retention and release behavior of aroma compounds is closely linked to MPs, the major structural proteins in skeletal muscle [4]. MPs consist of a complex mixture of contractile proteins, primarily myosin and actin. Myosin heavy chain (MHC) is the dominant protein in this mixture, known to undergo significant conformational changes in response to heat. Heat transitions can expose or shield reactive groups such as amino ($-NH_2$), thiol (-SH), and hydroxyl (-OH) groups, which can act as covalent binding sites for reactive aldehydes [5]. Notably, the binding capability of ligands is greatly influenced by the three-dimensional conformation of proteins in both covalent and non-covalent interaction patterns[6,7]. During heat

treatment, the spatial distribution of polar and nonpolar groups, steric hindrance, and binding cavities is altered by thermally induced conformational changes, thereby affecting the binding behavior of MPs-ligands. With numerous hydrophobic cores, MPs engage in non-covalent interactions, including hydrophobic interactions, hydrogen bonding, and van der Waals forces, with the flavor compounds[8]. The role of reversible non-covalent interactions in modulating binding behaviors under different treatment conditions contributes to dynamic binding equilibria. These interactions can influence the retention and release of volatile compounds without permanently altering protein structure [9]. In contrast, covalent interactions involve the formation of chemical bonds between reactive aldehydes and nucleophilic amino acid side chains, such as lysine or cysteine residues [10]. Typical reactions include Schiff base formation and Michael addition, particularly for α,β-unsaturated aldehydes [11]. Covalent modifications are more stable and may lead to irreversible structural alterations, potentially affecting protein functionality and nutritional properties. Moreover, the contribution of irreversible covalent adduct formation in modifying aroma perception requires highlighting (Table S1). Notably, a comprehensive evaluation that simultaneously considers both reversible non-covalent interactions and irreversible covalent adduct formation remains limited. This study addresses this gap by systematically providing novel mechanistic insights into the regulation of aldehyde binding behavior and aroma modulation. Mass spectrometry is a standard method to characterize covalent adducts by analyzing changes in molecular weight induced by covalent interactions of protein-ligand complexes. The covalent binding mechanisms observed between aldehydes and *β-lactoglobulin* included Schiff base formation and Michael addition, which may result in flavor loss [10]. Elucidation of the binding of MPs with flavors of different chemical structures provides a molecular basis for modulating meat flavor. We hypothesize that, as SBS undergoes processing at both boiling and low-temperature stewing, saturated and unsaturated aldehydes may modify MPs in a temperature-dependent manner, consequently affecting their

binding behavior. However, the temperature-dependent binding of aldehydes to MPs both covalently and non-covalently during thermal processing still needs to be investigated.

Given the above, the current study aimed to investigate the interactions between MPs and six ACs that vary in their carbon chain lengths and saturation degree. The binding affinities and interaction sites of six model ACs—hexanal (HE), octanal (OC), nonanal (NO), (E)-2-undecenal (UD), (E)-2-decenal (DE), and (E, E)-2,4-decadienal (DD)—with MPs were analyzed through molecular docking to elucidate differences in binding behavior. Liquid chromatography–mass spectrometry (LC-MS) was used to elucidate covalent binding sites in the interactions between ACs and MPs. Furthermore, the thermodynamic parameters and associated conformational changes of structurally diverse ACs toward MPs were also assessed. Overall, this work contributes to the understanding of the non-covalent and covalent interaction mechanisms between ACs and MPs, offering insights into the quality maintenance and flavor control of meat products

2. Results

2.1. Total sulfhydryl content

Total sulfhydryl (-SH) content reflects the abundance of cysteine residues in MPs and serves as an indicator of their modification by aldehyde compounds[12]. As shown in Fig.1-(A), a significant ($P < 0.05$) reduction in total sulfhydryl content was detected in MPs treated with the long-chain unsaturated aldehydes, including DE, UD, and DD. The reduction of total sulfhydryl was attributed to the covalent modification of protein thiol groups via Michael addition or thiol-aldehyde condensation[13]. These three aldehydes, with α, β-unsaturated carbonyl moieties, render the β-carbon highly electrophilic[14]. Consequently, the nucleophilic thiolate anions (S^-) from cysteine residues in MPs readily attack this electrophilic site, forming stable Michael adducts. In contrast, saturated aldehydes (HE, OC, NO) increased total

sulfhydryl content. Furthermore, the enhancement effect became more pronounced with prolonged heating. Saturated aldehydes, lacking conjugated double bonds, mainly interact with thiols through reversible reactions such as hemithioacetal formation[15]. With thermal denaturation of MPs, intramolecular hydrogen bonds and tertiary packing were disrupted, as well as cysteine residues that were originally buried within hydrophobic regions or involved in disulfide linkage were exposed. The hydrophobic nature of saturated aldehydes might further destabilize the native conformation of MPs and promote additional thiol exposure.

2.2. Free amine content

To assess protein oxidative injury and structural instability, the free amine content was quantified to elucidate changes in the ε-NH_2 groups of lysine side chains[16]. According to Fig.1.-(B), for the UH group, the free amine content of saturated aldehydes such as HE and OC significantly ($P < 0.05$) decreased due to Schiff base formation with lysine ε-amino groups [17]. In contrast, unsaturated aldehydes (UD, DE, and DD) induced a significant growth in free amine content ($P < 0.05$). Steric hindrance and hydrophobic interactions can be attributed to the observed variations. As shown in Fig.1.-(B), protein unfolding at elevated temperatures disrupted the tertiary structure of MPs, leading to the exposure of lysine residues. For the HU group, the free amine content of HE, DD, and UD showed a significant increase. While for the CD group, DE treatment enhanced the free amine content. Regarding unsaturated aldehydes, a dynamic equilibrium between Michael addition and Schiff base formation was established during heating, which influenced the changes in free amine content [18]. For HE, its relatively high volatility at high temperature may reduce the effective concentration participating in Schiff base formation.

2.3. Changes in secondary structure of MPs

The assessment of protein conformational changes was commonly carried out using circular dichroism. The secondary structure alterations of MPs combined with aldehydes were

investigated in the range 190–260 nm. As illustrated in Table 1, there was a significant decrease in the α-helix content, whereas the random coil content showed an increase. Extension of MPs caused by heat treatment resulted in partial unfolding of the molecular structure. After heat, the intramolecular hydrogen bonds along the peptide chains - which primarily stabilize α-helix structures - were progressively disrupted [19,20]. Consequently, a heat-induced structural transition from α-helix to random coil occurred. Besides, unsaturated aldehydes exhibited a more pronounced impact than saturated ones in the UH group, likely due to their differences in Schiff base formation, which could influence the inter-strand hydrogen bonds and disulfide bonds[21,22]. Furthermore, the addition of unsaturated aldehydes led to a rearrangement after prolonged stewing.

2.4. Surface hydrophobicity

The surface alterations of MPs were analyzed using surface hydrophobicity. As displayed in Fig.1.-(C), the surface hydrophobicity of MPs typically increased and then decreased during thermal processing. The initial increase resulted from heat-induced unfolding of the tertiary and secondary structures, exposing hydrophobic amino acid side chains[23]. However, after boiling, the subsequent decline of surface hydrophobicity in the CD group was observed, wherein exposed hydrophobic residues become reburied within protein clusters during stewing. Besides, disulfide bond formation further reduced surface hydrophobicity by promoting covalent compaction of protein structures[24]. Furthermore, the synergistic effect of aldehydes and heat on surface hydrophobicity was more obvious in the HU group. It's worth noting that the addition of DD significantly decreased the BPB content of MPs. Some reports demonstrated that the exposure of nonpolar amino acids and covalent cross-linking, such as nucleophilic addition with hydrophobic amino acids, may be attributed to the decline of surface hydrophobicity[25,26]. Additionally, the observed trend in surface hydrophobicity was consistent with increasing alkyl chain length. This was likely due to longer alkyl chains enhancing

hydrophobic interactions, promoting greater exposure of hydrophobic patches.

2.5. Fluorescence spectroscopy

To clarify the fluorescence quenching mechanism between aldehydes and MPs, the quenching behavior was analyzed using the Stern–Volmer model. As shown in Table 2 and Fig. 1-(D, E), the obtained Kq value was considerably higher than 2.0×10^{10} L·mol^{-1}·s^{-}, suggesting that the quenching process was mainly static rather than dynamic[27]. Static quenching occurs due to the formation of a ground-state complex between aldehydes and MPs rather than from collisional encounters during molecular diffusion[28]. Additionally, the calculated n values were approximately 1, indicating that MPs possess a single binding site for aldehydes [29]. Fluorescence quenching analysis indicated that MPs interact with the HE at multi-site binding modes ($n \approx 3$), suggesting multiple accessible residues contribute to the interaction [30]. These results reveal that the protein can accommodate multiple aldehyde molecules simultaneously, providing insight into the molecular basis of protein–aldehyde interactions relevant to flavor formation and protein modification [31]. To find out the binding forces between aldehydes and MPs, the thermodynamic parameters were determined. The negative ΔG values implied that the interaction between aldehydes and MPs can be classified as a spontaneous exergonic interaction[27]. The formation of HE-MPs was mainly driven by Van der Waals and hydrogen binding ($\Delta H < 0$ and $\Delta S < 0$). However, the positive ΔH and ΔS values suggested that the binding of OC, NO, DD, DE, and UD with MPs is mainly driven by hydrophobic interactions[32]. The thermodynamic analysis revealed distinct energetic profiles for different aldehydes, with evidence suggesting that hydrophobic interactions play a significant role. However, the complexity of the myofibrillar protein system and the potential for enthalpy-entropy compensation caution against oversimplified classification of binding forces. These phenomena can be inferred that aldehydes have long aliphatic chains, which make them highly hydrophobic. Consequently, they could easily be inserted into the non-polar parts of MPs.

2.6. Protein profiles

SDS-PAGE analysis was further used to evaluate the degradation and aggregation behavior under different thermal and aldehyde treatments. MPs primarily consisted of myosin heavy chain (MHC), myosin light chain (MLC), as well as actin (Fig.2), with band assignments according to Wang et al. [7]. After the addition of aldehydes, a decrease in MHC was observed, suggesting that aldehydes accelerated protein denaturation[4]. In the absence of β-mercaptoethanol (β-ME), the MHC bands of saturated aldehydes appeared lighter compared to those of unsaturated ones (Fig.2-(A)). This phenomenon was due to the Schiff bases between the aldehyde groups and the amino residues of the MHC, such as the thiol group[33]. A molecular weight aggregate formed as a result of covalent cross-linking and the MHC. Furthermore, as shown in Fig. 2-(A), with increasing chain length, the intensity of the MHC band increases gradually. Due to their smaller molecular size and higher accessibility to reactive amino groups, short-chain saturated aldehydes tend to induce more efficient cross-linking than long-chain ones. Besides, it's obvious in Fig.2-(C) that the MLC band became lighter in the CD group. In contrast, when β-ME was added, the disulfide bonds broke down, resulting in significantly darker protein bands. The presence of bands above the MHC suggests the presence of covalent adductions in a form other than disulfide bonds, such as Schiff base. The weakened bands, such as MHC and actin, observed after heating can be explained by thermally induced peptide degradation. Interestingly, deep MHC and actin bands were shown in Fig.2-(F), indicating structural rearrangements occurred in the CD group during the low-temperature heating. During this low-temperature cooling process, unsaturated aldehydes may act as 'molecular scaffolds' that limit random aggregation. The steric hindrance and rigid molecular geometry imposed by α, β-unsaturated aldehydes were reported to modulate protein–ligand aggregation [34]. Consequently, the band recovery was more pronounced for unsaturated aldehydes than for saturated aldehydes.

2.7. Particle size

To examine changes in protein aggregation following aldehydes and heat treatment, particle sizes were measured and shown in Fig. 3-A. For the UH group, the addition of aldehydes increased in particle size, indicating the formation of aggregates. The covalent cross-links or Schiff bases formation might be the main promoters influencing intermolecular aggregation. It was evident from the CK group that, in the absence of aldehydes, heating induced significant protein aggregation and larger particle sizes. The results revealed that thermal treatment caused rapid aggregation and the formation of large protein clusters. Interestingly, for the CD group, the addition of aldehydes decreased particle size during lengthy heating. The covalent binding of aldehydes, such as Schiff bases and Michael additions, partially occupied the reactive amino groups and restricted the random rearrangement. Besides, hydrophobic aldehydes can enter nonpolar regions, increasing steric hindrance and preventing excessive hydrophobic interactions between proteins[35]. Subsequently, thermally induced large protein aggregation was restricted, and MPs tend to form smaller compact particles. Moreover, consistent with a previous study[35], the restrictive effect was much more evident in the presence of unsaturated aldehydes, particularly those with conjugated double bonds. This phenomenon can be attributed to their α, β-unsaturated structure, which allows for both Schiff base reactions and Michael addition reactions with nucleophilic groups, hence preventing excessive intermolecular cross-linking and uncontrolled aggregation[36].

2.8. Microstructures of MPs

AFM was used to further analyze the microstructural changes after the treatment of aldehydes and heat treatment. As shown in Fig.3-(B), in the absence of aldehydes, the untreated MPs exhibited a typical flat and uniform surface, which indicated that the microstructure of MPs was stable and well-dispersed. However, aldehyde treatment resulted in obvious irregular aggregation, height increase, and undulations. This can be attributed to the ability of aldehydes

to penetrate protein nonpolar regions, thereby increasing steric hindrance and facilitating the formation of larger aggregates. Besides, covalent Schiff base formation between aldehydes and either the ε-amino groups of lysine or the thiol groups of cysteine could promote intermolecular crosslinking and induce clustered aggregation[4]. Besides, it was shown in Fig.3-(B) that the initial spherical MP particles transformed into a loose and irregular surface with heating. Interestingly, heating with the addition of DD produced smaller particles that were more uniformly distributed and had relatively smooth surfaces. This observation aligns with particle size results (Fig.3-(A)). The special conjugated diene structure of DD, which makes it more electrophilic than saturated aldehydes and monounsaturated aldehydes, might be reasonable for this phenomenon. On the one hand, while all aldehydes can form Schiff bases with lysine ε-amino groups, DD were much easier to undergo Michael addition with nucleophilic residues such as cysteine and histidine for their conjugated double bonds (Table 3). These dual reaction pathways limited excessive protein–protein crosslinking and prevented the development of large insoluble aggregates. Previous studies have confirmed that DD induces side-chain modifications and conformational changes in proteins, leading to altered aggregation[36,37]. On the other hand, the medium-chain hydrophobic tail and rigid, conjugated structure of DD promote its insertion into the nonpolar domains of unfolded proteins[4]. In that way, steric hindrance limited excessive protein–protein hydrophobic stacking. This covalent and non-covalent binding could be responsible for the modulation of thermal protein aggregation and unfolding.

2.9. Verification of the type of interactions between MPs and aldehydes

The chemical structures and functional groups of aldehydes regulated their interactions with MPs. The specific contributions of these non-covalent and covalent forces were probed using bond-disrupting agents ($Cl_3CCOONa$, GuHCl, Na_2SO_4, PG, Urea, and DTT)[38]. Table S3 lists the effects of various reagents on the molecular interaction of MPs. As shown in Fig.4-

(A), the non-covalent interactions among HE, OC, NO, DD, UD, and DE to MPs may primarily be dominated by hydrophobic interactions, hydrogen bonding, and electrostatic interactions. For HE, a significant increase was detected with the addition of $Cl_3CCOONa$, which destabilized protein structure, resulting in the release of the aldehyde[31]. However, the outcomes for the other two saturated aldehydes were different. OC and NO exhibited increases in peak area with Na_2SO_4, GuHCl, and PG. During salt-induced aggregation caused by Na_2SO_4, aldehydes that are initially bound in hydrophobic pockets may be displaced into the aqueous phase. As a result, their headspace concentration increased. The disrupting agent, such as GuHCl and PG, weakened the hydrophobic interactions, thus elevating the headspace concentration of OC and NO. This was consistent with the measurements of the thermodynamic parameters (Table 2). The binding of OC and NO to the MPs is primarily driven by hydrophobic interactions. Notably, DD and DE showed similar decreases across different disturbing agents, which might result from the formation of stable covalent adduction. The binding behavior between aldehydes and MPs at different concentrations was displayed in Fig. 4-(B). The cluster analysis under varying thermal treatments and concentrations revealed two distinct interaction patterns: saturated and unsaturated aldehydes. In comparison, saturated aldehydes exhibited a more pronounced binding effect at low concentrations, whereas unsaturated aldehydes demonstrated stronger binding at higher treatment levels. This discrepancy can be attributed to their distinct chemical reactivity and interaction mechanisms with proteins. Saturated aldehydes primarily interact through reversible non-covalent forces, such as hydrophobic interactions and hydrogen bonding [11]. At low concentrations, the number of available binding sites on the protein is greater than the number of ligand molecules. This results in efficient sequestration and a noticeable reduction in headspace concentration. However, as the concentration increases, these interactions tend to approach saturation, leading to a diminished incremental binding effect. In contrast, unsaturated aldehydes—particularly

α,β-unsaturated aldehydes—possess electrophilic carbon–carbon double bonds that enable covalent reactions (e.g., Schiff base formation and Michael addition) with nucleophilic amino acid residues [11]. At lower concentrations, the extent of these reactions may be limited by reaction kinetics; however, at higher concentrations, the probability of collision and covalent modification increases substantially, resulting in a more significant binding effect. Further analysis, such as molecular docking and proteomics, was used to analyze the non-covalent and covalent binding behavior.

2.10. Molecular docking

Molecular docking was applied to elucidate the non-covalent interactions between aldehydes and MPs. Previous studies have demonstrated that hydrophobic interaction and hydrogen bonding sites within protein cavities are crucial contributors to ligand-protein complex stabilization[39]. The binding energies and sites were presented in Table S4 and Fig.4-(C). The negative binding energies indicated that the interactions between aldehydes and MPs were thermodynamically favorable[6]. The stabilization of complexes was largely due to hydrogen bonds, in which ASN187 was identified as a critical binding residue. Besides, as shown in Fig.4-(B), the terminal regions of α-helices in myosin could potentially act as binding sites for aldehydes. The structure of those regions was flexible, which resulted in partially exposed hydrophobic residues such as leucine, isoleucine, and valine. These nonpolar pockets can bind aliphatic aldehydes, with the strength of the bond increasing with the chain length. It can be seen that longer-chain unsaturated aldehydes, such as DD, UD, and DE, can penetrate better into hydrophobic pockets, which is in accordance with the research of Snel et al.[35]. By contrast, HE, as a short and saturated chain aldehyde, showed the lowest binding energy. In accordance with the result of fluorescence quenching, HE is less capable of occupying nonpolar protein cavities due to its weaker hydrophobicity (Table S1). Furthermore, its smaller molecular volume may also limit steric complementarity with hydrophobic pockets, further

reducing binding stability. In addition, the binding energies of longer-chain unsaturated aldehydes were not higher than those of saturated aldehydes as hypothesized. This was likely due to the fact that the ability to conform to the hydrophobic pocket was limited by steric hindrance.

2.11. Covalent binding between aldehydes and MPs

The covalent modification sites on MPs for aldehydes were elucidated using LC-MS/MS [40]. Covalent modification sites for both Schiff base and Michael addition were identified and listed in Table 3 and Fig.S2. A total of 23 modified peptides were identified, with HE, OC, NO, DD, DE, and UD modifying 2, 1, 1, 17, 1, and 1 peptides, respectively. Myosin was the predominant target, accounting for 10 modified peptides from MHC and MLC. This finding is consistent with the SDS-PAGE results. Saturated aldehydes, especially HE, predominantly undergo Schiff base reaction. Schiff base reaction was predominantly found at Lys and Arg residues. This was consistent with earlier studies showing that aldehydes react with the nucleophilic ε-amino groups of Lys residues [10,41]. Besides, saturated aldehydes exhibited lower reactivity as chain length increased, which can be attributed to enhanced steric hindrance. While unsaturated aldehydes mainly participated in Michael addition at His, Cys, Lys, Trp, and Arg residues. The conjugated double bond systems of α, β-unsaturated resulted in their stronger electrophiles, which enhanced Michael addition with nucleophilic residues, including cysteine thiols and histidine imidazoles. This was consistent with the results of sulfhydryl content. Besides, both covalent and non-covalent bonds influence each other. The hydrophobic tail and rigid conjugated structure of DD promoted its insertion into MPs, proteins, thereby reducing the distance to covalent binding sites[11]. Covalent binding can influence the flavor perception by altering the release of aldehydes as well as the structure and surface of MPs[10]. Usually, the covalent binding decreases the volatility and sensory intensity due to the irreversible binding.

3. Discussion

K-means clustering was used to reveal how saturated and unsaturated aldehydes interact with MPs under stage-thermal regimes. K-means clustering enabled the identification of structural and thermodynamic patterns among different aldehydes without predefined classification criteria. This data-driven grouping revealed consistent trends related to aldehyde structure (saturated vs. α,β-unsaturated) and binding behavior, supporting the proposed structure–reactivity relationship. As shown in Fig.5, HU was a distinct group characterized by increasing surface hydrophobicity and exposure of reactive sites and partial unfolding of secondary structures. Under extended LTLT stewing, extensive aggregation and refolding reduce accessible binding sites. This is consistent with observed decreases in hydrophobic interaction strength after prolonged thermal exposure. According to our results, the non-covalent and covalent mechanisms for the impact of structural characteristics on aldehyde binding are presented in Fig.6. Aldehydes can covalently modify the MHC and MLC through Schiff base and Michael addition. Saturated aldehydes, such as HE, OC, and NO, readily reacted with the ε-NH_2 groups of lysine side chains through Schiff base formation. However, unsaturated aldehydes, especially α,β-unsaturated aldehydes, preferentially participated in Michael addition reactions with cysteine thiol groups. In addition to covalent interactions, non-covalent interactions also play a crucial role in forming the MPs-aldehyde complex [11]. Beyond these covalent interactions, non-covalent forces (e.g., hydrophobic interactions, hydrogen bonding) also contributed significantly to the formation of the myofibrillar protein (MP)-aldehyde complex. Fluorescence quenching analysis revealed that shorter-chain aldehyde (HE) was primarily stabilized by hydrogen bonding, while long-chain and unsaturated aldehydes predominantly bound via hydrophobic interactions. A comparable mechanism was observed where hydrophobic interactions have been identified as the primary driving force for MPs-aldehyde interaction[31]. Notably, (*E, E*)-2,4-decadienal had the greatest number of covalent binding sites. Meanwhile, the hydrophobic tail and rigid, conjugated structure of (*E, E*)-2,4-

decadienal facilitate its insertion into MPs, thereby reducing its distance to covalent binding sites. That is, both covalent and non-covalent interactions influence each other mutually, jointly regulating their binding and release from MPs. The binding would change during the heat processing in accordance with the variation of the protein's degree of deformation. As heating disrupted intermolecular hydrogen bonds, a substantial decrease in β-sheet content was observed. Conversely, the relative stability of the α-helix was maintained by the relatively stable intramolecular hydrogen bonds. Molecular docking results indicated that aldehydes interacted with regions of the α-helix where hydrophobic residues were exposed, such as leucine, isoleucine, and valine. Boiling (HU treatment) promoted the unfolding of secondary and tertiary structures, thereby resulting in exposure of hydrophobic side chains and facilitating aldehyde binding. Meanwhile, the presence of aldehydes acted synergistically with heating to promote exposure of hydrophobic regions, particularly for long-chain aldehydes, whose alkyl tails intensified hydrophobic interactions. However, after low-temperature stewing (CD treatment), the exposed hydrophobic residues tended to rearrange and re-bury within protein clusters, thereby reducing surface hydrophobicity. In accordance, particle size and AFM results showed that the addition of aldehydes effectively restricted random aggregation during stewing, resulting in a more uniform size distribution and a smoother surface compared with control groups. During stage heating, the aldehydes-MPs complex has a large influence on the sensory profile of SBS. It is imperative to acknowledge that the focal point of this study was protein-flavor binding under controlled in vitro conditions. While these interactions are likely to influence flavor retention during processing, the direct correlation with sensory perception during consumption remains to be established. In order to validate the sensory relevance of these molecular interactions, further studies are required. Such studies should include simulated oral release experiments or sensory evaluation. Typically, covalent binding can reduce the volatility of ACs, diminishing their contribution to sensory impact, such as green or fatty. In

contrast, non-covalent interactions can affect flavor release during consumption. Different from covalent binding, non-covalent binding irreversibly influences the rate and extent of volatile liberation. The rearrangement of MPs at the long-time stewing prolongs aroma persistence and improves flavor stability. Non-covalent modifications may contribute dynamically to flavor release during storage. While covalent binding, such as Michael adducts, provides more persistent covalent modifications that could impact both flavor retention and protein functionality. Besides, the extent and sensory consequences of these bindings are greatly influenced by the chemical structure of ACs, the amino acid composition of the MPs, and processing conditions could influence both types of interaction.

This study investigated the covalent and non-covalent interaction mechanisms between MPs and six aldehydes that differ in carbon chain length and degree of saturation. High temperature increased protein denaturation, while subsequent low-temperature stewing displayed protein rearrangement. Typically, aldehyde treatment increased the irregular thermal aggregation of protein due to its steric hindrance. However, DD, with a special rigid conjugated diene structure, prevented protein aggregation during heating, resulting in smaller particles. The formation of HE-MPs was primarily driven by hydrogen bonding, while longer-chain or unsaturated aldehydes penetrated hydrophobic pockets more effectively. Saturated aldehydes (HE, OC, and NO) were found to be primarily engaged in Schiff base reactions with the lysine ε-amino group. By contrast, α, β-unsaturated aldehydes (UD, DE, and DD) exhibited greater electrophilicity, participating extensively in Michael addition with nucleophilic residues such as cysteine, histidine, and tryptophan, as well as forming Schiff bases. Therefore, the retention/release of flavor is determined by covalent and non-covalent bonds together. Identification of specific protein conformational states during heat processing as key flavor carriers plays a vital role in determining the long-term evolution of flavors. Future research should focus on quantifying the relationship between MPs-ACs binding behavior and flavor

sensory impact. The results can be useful to investigate complex ACs, such as pyrazines, furans, and thiazoles, to optimize meat flavor profiles while minimizing quality deterioration in meat products. Moreover, the characterization of Schiff base and Michael adduct formation provides a framework for future studies investigating protein–aldehyde interactions, including their impact on protein functionality, flavor retention, and nutritional quality. Future research endeavors may entail the integration of sensory evaluation, oxidative stability assays, and molecular modeling to enhance the comprehension and regulation of flavor formation in meat and other protein-rich foods. Controlling oxygen exposure, storage temperature, and antioxidant strategies may help regulate aldehyde formation to optimize sensory quality while minimizing oxidative damage. This balanced perspective provides practical implications for meat processing and quality management. Such research will establish a fundamental flavor control framework for developing precision industrial processing technologies.

4. Methods

4.1. Materials

Fresh beef (*longissimus thoracis et lumborum*) was obtained from a local supermarket (slaughter ages 22–24 months, slaughter weights 350–400 kg, the carcasses were aged at 4 °C). Aldehyde compounds: HE, OC, NO, UD, DE, and DD were purchased from Sigma-Aldrich Chemical Co., Ltd (Shanghai, China). Other chemicals were analytical grade from Sinopharm Chemical Reagent Co., Ltd. (Shanghai, China). The physicochemical properties of aldehydes were presented in Table S1.

4.2. Extraction of myofibrillar proteins (MPs)

MPs were extracted using a modified version of the method described by[7]. Briefly, minced muscle tissue was homogenized in phosphate extraction solution (PES: 0.1 M NaCl, 1 mM EGTA, 2 mM $MgCl_2$, 10 mM $Na_3PO_4 \cdot 12H_2O$, pH 7) at 12,000 rpm for 15 s (three times,

with 15s intervals). The resulting homogenate was then centrifuged at 3,000 × g (4 °C, 15 min). After centrifugation, the pellet was washed twice under the same conditions and then underwent three additional washes with a 0.1 M NaCl solution. The MPs were stored at 4 °C within 48 h. Before further analysis, the MPs were diluted to the desired concentration using pre-chilled phosphate buffer solution (PBS: 20 mM Na_2HPO_4 and 0.6 M NaCl, pH 7.0). Protein concentration was determined using a bicinchoninic acid (BCA) protein assay kit (Solarbio, Beijing, China).

4.3. Preparation of heated MPs

The concentration was diluted to 4 mg/mL with PBS. The protein solution was divided equally into 21 aliquots, which were randomly numbered 1–21 for different treatments (three heating levels: UH: unheated, HU: heat up, boiled to 85°C and left for 10 min; CD: cool down, boiled to 85°C, left for 10 min, and then simmered at 45°C for 30 min) × 6 aldehydes (HE, OC, NO, DD, DE, UD) + 3 control (UH, HU, CD). The heating parameters were selected to emulate the heating rate employed in industrial processing, as demonstrated in the temperature monitoring curve presented in (Fig.S1). The 1 mM aldehyde concentration was selected based on its alignment with the upper range of concentrations reported in industrial SBS production [1]. After heating, the samples were promptly cooled in ice water and then stored in a refrigerator at 4℃ for further analysis.

4.4. Protein surface hydrophobicity, total sulfhydryl, and free amine groups determination

Surface hydrophobicity was calculated using the method described by [27]. The test group (1 mL of 2 mg/mL MPs) and the control group (1 mL of PBS) were mixed with bromophenol blue (BPB, 200 μl of 1 mg/mL) and then vortexed for 30 s. This mixture was then shaken at 25 ± 1 °C for 15 min, followed by centrifugation at 4000×g for 15 min, at 25 °C. And then, 1 mL of the supernatant was diluted with 9 mL of PBS. The absorbance measurement was recorded

at 595 nm. Surface hydrophobicity was calculated based on the amount of bound BPB as shown in Eq. (1):

$$\text{Bound BPB (μg)} = 200 \times \frac{OD_{ck} - OD_{MPs}}{OD_{ck}} \quad (1)$$

OD_{ck} and OD_{MPs} were the respective differences in absorbance at 595 nm between the blank and experimental groups.

The total sulfhydryl content of MPs was calculated using the DTNB method [32]. The protein solution was measured at 412 nm with an extinction coefficient of 13,600 M^{-1} cm^{-1}. Free amine groups (FAG, nmol/mg protein) were determined using TNBS following the method of Wang et al.[11]. Absorbance was measured at 420 nm, and the FAG content was quantified using a calibration curve generated with L-leucine.

$$SH\left(\frac{\mu mol}{g} protein\right) = \frac{A_{412} \times 10^6}{13{,}600 \times l \times C} \quad (2)$$

where $A_{412}$is the absorbance at 412 nm, $l$is the optical path length (1 cm), and $C$is the protein concentration (g/mL).

4.5. The secondary structures analysis by circular dichroism spectroscopy

The MOS-450/AF-CD spectrometer (Bio-Logic, France) was utilized to capture the circular dichroism spectroscopy of the MPs (0.5 mg/mL) in accordance with a method previously described [6]. Spectra were collected across a wavelength range of 190–260 nm. The secondary structures of the MPs, such as α-helices, β-sheets, β-turns, and random coils, were calculated using the DichroWeb platform[42].

4.6. The quenching mechanism analysis by fluorescence spectroscopy

The experiments were conducted in accordance with the methodology described by Bortnowska[27], with minor modifications. A solution of MPs (0.5 mg/mL) was prepared by diluting with 20 mM PBS. Solutions of aldehydes were added individually to vials containing the MP solution, achieving final concentrations ranging from 0 to 1.25 mM. After incubation at different temperatures (298K, 303K, and 310K), fluorescence spectra were collected in the

range of 310–450 nm excitation at 280 nm with a fluorescence spectrophotometer (BioTek Synergy H1, Agilent Technologies, Inc., California, USA). The quenching mechanism of aldehydes on MPs' fluorescence was evaluated using the Stern–Volmer equation, as shown in Eq. (3):

$$\frac{F_0}{F} = 1 + K_{SV}[Q] = 1 + K_q\tau_0[Q] \quad (3)$$

F_0 and F, different fluorescence intensities without and with the quencher; K_{SV}, the Stern–Volmer quenching constant; [Q], aldehyde concentration; K_q, the bimolecular quenching rate constant; and τ_0 (10^{-8} s), the average fluorescence lifetime of MPs in the absence of quencher.

Besides, the binding constant (K_b) and binding site number (n_b) were calculated using the double logarithm equation, as shown in Eq. (4):

$$\log[\frac{(F_0-F)}{F}] = \log K_a + n\log[Q] \quad (4)$$

Furthermore, the thermodynamic parameters, including enthalpy change (ΔH), entropy change (ΔS), and Gibbs free energy (ΔG), were estimated from the Eq. (5) and (6):

$$\ln K_a = -\frac{\Delta H}{RT} + \frac{\Delta S}{R} \quad (5)$$

$$\Delta G = \Delta H - T\Delta S \quad (6)$$

R, the gas constant (8.314 $J\cdot mol^{-1}\cdot K^{-1}$); T, the absolute temperature (K).

4.7. Particle size

The mean particle size (Z-average) was measured using a Zetasizer Nano-ZS (Malvern Instruments, Malvern, Worcestershire, UK) instrument at 25 °C. MPs solutions (1 mg/mL) were dispersed in 50 mM phosphate buffer (pH 7.0, containing 0.6 M NaCl) were analyzed at a scattering angle of 90°. Measurements were conducted with the relative refractive index set at 1.414 and the absorption index set at 0.001.

4.8. Sodium dodecyl sulfate-polyacrylamide gel electrophoresis (SDS-PAGE).

MPs solutions (2 mg/mL) were combined with an equal volume of Laemmli buffer and

heated at 100 °C for 5 min. The mixture was centrifuged at 15,000×g for 15 min at 4 °C. Then, 10 μL supernatant and 5 μL of standard markers were loaded onto a 12.5% precast polyacrylamide gel. After separation, gels were stained with Coomassie Blue R-250 and then destained. Band quantification was performed using Quantity One software, with molecular weights and relative contents determined by comparison to the unheated control.

4.9. Chemical bonds

Guanidine hydrochloride (GuHCl, disrupting hydrophobic interactions, hydrogen bonding, and ionic effects), propylene glycol (PG, suppressing hydrophobic forces while enhancing hydrogen bonding), urea (disrupting hydrophobic interactions and hydrogen bonding), $Cl_3CCOONa$ (destabilizing protein structure), and DTT (reducing inter- and intramolecular S–S bonds) were used to probe interaction mechanisms [27]. Volatile compounds were extracted using a divinylbenzene/ carboxen/ polydimethylsiloxane (DVB/CAR/PDMS) fiber at 25 °C for 30 min, followed by desorption in the GC injector at 250 °C for 3 min. Volatile compounds were analyzed on an Agilent 8860 GC-MS system equipped with a DB-Wax column (30 m × 0.18 mm × 0.18 μm). The oven temperature was programmed from 35 °C (hold 3 min) to 210 °C at 5 °C/min. Mass spectrometric analysis was operated in electron impact (EI) mode at 70 eV, with the ion source temperature set at 230 °C and scanning from m/z 35 to 400.

4.10. Binding behavior

The protein-aroma binding ability was determined in accordance with the method established by Wang et al.[43]. Stock solutions of the aldehydes were prepared by dissolving each compound in methanol to a final concentration of 10 mM. These solutions were subsequently incorporated into both the myofibrillar protein (MPs) solution (4 mg/mL) and the control solution (20 mM PBS) to attain a series of final aroma compound concentrations (0, 0.01, 0.02, 0.04, 0.08, 0.16, 0.2, 0.4, 0.6, 0.8, and 1 mM). An aliquot (5 mL) of each mixture was

transferred into a 20 mL headspace vial, which was then sealed with a PTFE-lined silicone septum. The vials were stored at 4 °C for 12 h to allow equilibration. Contents of aldehydes were determined as described in 4.5.1.

4.11. Atomic force microscopy (AFM)

An aliquot (10 μL) of each aldehyde-MPs complex (0.25 mg/mL) was deposited onto a freshly cleaved mica surface and air-dried to form a thin film under ambient conditions.

4.12. Molecular docking

The crystal structure of myosin (PDB ID: 8QYU) was obtained from the RCSB Protein Data Bank. The three-dimensional structures of the selected flavor compounds were retrieved from the PubChem database. Molecular docking simulations were carried out using AutoDock Vina. The Autodock Vina binding pocket was selected by PyMOL (x=-38.4; y=-13.9; z=12.8). This globular region is the primary site for small hydrophobic ligand binding due to its structural flexibility and the presence of hydrophobic pockets. The optimal conformation for each protein–ligand pair was identified through a comprehensive analysis of the Vina scoring function, followed by a meticulous examination of the resulting interaction patterns. The visualization and analysis of hydrogen bonds, hydrophobic contacts, and key interacting residues were conducted with the use of LigPlus and PyMOL.

4.13. Proteomics analysis

The heated aldehyde-MPs solution was washed twice with NH_4HCO_3 (200 μL of 50 mM) buffer solution and then centrifuged (12,000 rpm, 5 min). Samples were alkylated with 5 μL of iodoacetamide for 1 h, subsequently undergoing tryptic digestion at 37 °C for 16 h (enzyme-to-protein ratio 1:50, w/w). The digestion was quenched with 2 μL of 1% formic acid, and the peptides were analyzed by LC-MS/MS. The MS/MS spectra were then searched against the UniProt database using Proteome Discoverer 2.4.

4.14. Machine learning analysis

Following the theoretical framework of clustering algorithms proposed in previous research[44], the K-means algorithms were applied to categorize the binding behavior of aldehydes. Clustering models were constructed and visualized using MetaboAnalyst 6.0. K-means clustering was performed to group the samples based on protein structure changes. Prior to clustering, all features were standardized using z-score normalization. The optimal number of clusters (k) was determined using the elbow method and validated with silhouette scores.

4.15. Statistical analysis

All experiments were carried out in triplicate. The data were presented as the mean ± standard error (SE) and were analyzed using one-way ANOVA and generalized estimating equations in IBM SPSS Statistics 26.0.

Data availability

The datasets generated and analyzed during the current study are not publicly available but are available from the corresponding author on reasonable request.

Acknowledgements

This study was supported by the Agricultural Science and Technology Innovation Program (ASTIP-Y2025QC29), the National Natural Science Foundation of China (No. 32472392), and the China Scholarship Council.

Author Contributions

Jingfan Wang: Writing - original draft, Formal analysis, Conceptualization, Investigation, Methodology, Data curation. Tianze Wang: Formal analysis, Investigation, Methodology. Ping Yang: Writing - review & editing. Dong Han: Writing - review & editing, Funding acquisition. Chunhui Zhang*:* Conceptualization, Funding acquisition, Writing - review & editing. Wei Jia:

Data curation. Giorgia Purcaro: Writing - review & editing. Marie-Laure Fauconnier: Writing - review & editing.

Competing interests

The authors declare no competing financial interest.

References

1. Wang, J. *et al.* Study of the flavor dissipation mechanism of soy-sauce-marinated beef using flavor matrices. *Food Chemistry* **437**, 137890 (2024).
2. Sohail, A. *et al.* Aroma compounds identified in cooked meat: A review. *Food Research International* **157**, 111385 (2022).
3. Bleicher, J., Ebner, E. E. & Bak, K. H. Formation and Analysis of Volatile and Odor Compounds in Meat—A Review. *Molecules* **27**, 6703 (2022).
4. Dou, P., Feng, X., Cheng, X., Guan, Q. & Chen, L. Binding of aldehyde flavour compounds to beef myofibrillar proteins and the effect of nonenzymatic glycation with glucose and glucosamine. *LWT- Food Science and Technology* **144**, 111198 (2021).
5. Lv, T. *et al.* Effect of trypsin treatments on the structure and binding capacity of volatile compounds of myosin. *Food Chemistry* **214**, 710–716 (2017).
6. Di, C. & Jia, W. Capture modes evaluation of four flavor constituents in β-lactoglobulin by high-resolution mass spectrometry and molecular dynamics simulation approaches. *Food Hydrocolloids* **145**, 109157 (2023).
7. Wang, T. *et al.* Binding of Selected Aroma Compounds to Myofibrillar Protein, Sarcoplasmic Protein, and Collagen during Thermal Treatment: Role of Conformational

Changes and Degradation of Proteins. *J. Agric. Food Chem.* https://doi.org/10.1021/acs.jafc.3c02618 (2023) doi:10.1021/acs.jafc.3c02618.

8. He, Y., Zhou, C., Li, C. & Zhou, G. Effect of incubation temperature on the binding capacity of flavor compounds to myosin. *Food Chemistry* **346**, 128976 (2021).
9. Zhang, J., Kang, D., Zhang, W. & Lorenzo, J. M. Recent advantage of interactions of protein-flavor in foods: Perspective of theoretical models, protein properties and extrinsic factors. *Trends in Food Science & Technology* **111**, (2021).
10. Anantharamkrishnan, V., Hoye, T. & Reineccius, G. A. Covalent Adduct Formation Between Flavor Compounds of Various Functional Group Classes and the Model Protein β-Lactoglobulin. *J. Agric. Food Chem.* **68**, 6395–6402 (2020).
11. Wang, T. *et al.* Unraveling the covalent binding mechanisms of aroma compounds with porcine proteins: A mass spectrometry, proteomics, and conformational analysis approach. *Food Chemistry* **493**, 145913 (2025).
12. Wang, K. & Arntfield, S. D. Modification of interactions between selected volatile flavour compounds and salt-extracted pea protein isolates using chemical and enzymatic approaches. *Food Hydrocolloids* **61**, 567–577 (2016).
13. Lund, M. N., Heinonen, M., Baron, C. P. & Estévez, M. Protein oxidation in muscle foods: a review. *Mol Nutr Food Res* **55**, 83–95 (2011).
14. Jackson, P. A., Widen, J. C., Harki, D. A. & Brummond, K. M. Covalent Modifiers: A Chemical Perspective on the Reactivity of α,β-Unsaturated Carbonyls with Thiols via Hetero-Michael Addition Reactions. *J Med Chem* **60**, 839–885 (2017).
15. Ouellette, R. J. & Rawn, J. D. Aldehydes and Ketones. in *Organic Chemistry* 629–657 (Elsevier, 2014). doi:10.1016/B978-0-12-800780-8.00019-X.

16. Chen, L. *et al.* Production of branched-chain flavor compounds from hydrolysis of pork myofibrillar protein by optimizing the inoculation of *Limosilactobacillus fermentum* YZU-06 and *Staphylococcus saprophyticus* CGMCC 3475. *LWT* **189**, 115512 (2023).

17. Wang, J., Zhao, M., Qiu, C. & Sun, W. Effect of malondialdehyde modification on the binding of aroma compounds to soy protein isolates. *Food Research International* **105**, 150–158 (2018).

18. Xu, L. *et al.* A structural explanation for enhanced binding behaviors between β-lactoglobulin and alkene-aldehydes upon heat- and ultrasonication-induced protein unfolding. *Food Hydrocolloids* **130**, 107682 (2022).

19. Ju, Q. *et al.* Heat-induced aggregation of subunits/polypeptides of soybean protein: Structural and physicochemical properties. *Food Chemistry* **405**, 134774 (2023).

20. Chen, H. *et al.* Exploring in vitro gastrointestinal digestion of myofibrillar proteins at different heating temperatures. *Food Chemistry* **414**, 135694 (2023).

21. Dockal, M., Carter, D. C. & Rüker, F. Conformational Transitions of the Three Recombinant Domains of Human Serum Albumin Depending on pH*. *Journal of Biological Chemistry* **275**, 3042–3050 (2000).

22. Hendy, A. *et al.* Enhancement of biological properties in casein protein through functionalization with cinnamaldehyde via Schiff base bonding: antibacterial and antioxidant effects. *RSC Adv.* **15**, 27300–27310 (2025).

23. Kobayashi, Y., Mayer, S. G. & Park, J. W. Gelation properties of tilapia fish protein isolate and surimi pre- and post-rigor: Rigor condition of tilapia FPI and surimi. *Food Bioscience* **17**, 17–23 (2017).

24. Cao, H. *et al.* Microwave irradiation promotes aggregation behavior of myosin through conformation changes. *Food Hydrocolloids* **96**, 11–19 (2019).

25. Zhou, F., Zhao, M., Cui, C. & Sun, W. Influence of linoleic acid-induced oxidative modifications on physicochemical changes and *in vitro* digestibility of porcine myofibrillar proteins. *LWT - Food Science and Technology* **61**, 414–421 (2015).

26. Yang, Q. L. *et al.* Effect of pH on the interaction of volatile compounds with the myofibrillar proteins of duck meat. *Poultry Science* **96**, 1963–1969 (2017).

27. Bortnowska, G. Aroma compounds retention and release from protein-polysaccharide-based bilayer emulsion gels: A thermodynamic and kinetic study. *Food Hydrocolloids* **150**, 109648 (2024).

28. Yu, Y. *et al.* Exploring the interaction between myofibrillar proteins and pyrazine compounds: Based on molecular docking, molecular dynamics simulation, and multi-spectroscopy techniques. *International Journal of Biological Macromolecules* **253**, (2023).

29. Rahman, N. *et al.* Multispectroscopic and molecular docking studies on the interaction of diltiazem hydrochloride with bovine serum albumin and its application to the quantitative determination of diltiazem hydrochloride. *Journal of King Saud University - Science* **34**, 102267 (2022).

30. Wei, M. *et al.* Investigating the interactions between selected heterocyclic flavor compounds and beef myofibrillar proteins using SPME-GC–MS, spectroscopic, and molecular docking approaches. *Journal of Molecular Liquids* **403**, 124878 (2024).

31. Bi, S. *et al.* Non-covalent interactions of selected flavors with pea protein: Role of molecular structure of flavor compounds. *Food Chemistry* **389**, 133044 (2022).

32. Bi, K. *et al.* Exploring the off-flavour removal mechanism of d-limonene, geraniol and acetophenone in perilla leaves from the perspective of molecular structure and kinetic properties. *Food Chemistry* **480**, 143938 (2025).

33. Li, C., Xiong, Y. L. & Chen, J. Oxidation-induced unfolding facilitates Myosin cross-linking in myofibrillar protein by microbial transglutaminase. *J Agric Food Chem* **60**, 8020–8027 (2012).

34. Yang, T. *et al.* Novel insights into interfacial effects on α, β-unsaturated aldehyde-induced modifications of milk proteins and polyphenol interventions in multiphase food systems. *Food Hydrocolloids* **172**, 111962 (2026).

35. Snel, S. J. E. *et al.* Flavor-protein interactions for four plant protein isolates and whey protein isolate with aldehydes. *LWT* **185**, 115177 (2023).

36. Li, W., Wu, Y., Li, C. & Zhu, L. Effect of (E,E)-2,4-decadienal on Side-Chain Modification, Conformation Change, and Aggregation of Bovine Serum Albumin. *European Journal of Lipid Science and Technology* **124**, 2100066 (2022).

37. Chu, Y., Ding, Z. & Xie, J. Molecular Mechanism of the Impact of Lipid Oxidation Products (2,4-Decadienal) on the Conformation of Grouper (Epinephelus coioides) Myofibrillar Proteins During Refrigeration and its Implications on the Overall Protein Flavor. *Food Bioprocess Technol* **17**, 5299–5311 (2024).

38. Wang, K. & Arntfield, S. D. Probing the molecular forces involved in binding of selected volatile flavour compounds to salt-extracted pea proteins. *Food Chemistry* **211**, 235–242 (2016).

39. Gong, S. *et al.* Study on the interaction mechanism of purple potato anthocyanins with casein and whey protein. *Food Hydrocolloids* **111**, 106223 (2021).

40. Anantharamkrishnan, V. & Reineccius, G. A. Influence of pH, Temperature, and Water Activity on Covalent Adduct Formation between Selected Flavor Compounds and Model Protein βLactoglobulin. *Journal of Agricultural and Food Chemistry* **68**, 13833–13843 (2020).

41. Yu, Y. *et al.* Spice aldehydes improve emulsification stability of β-carotene by Schiff base reaction binding sodium caseinate as emulsion surface stabilizer. *Food Chemistry* **475**, 143305 (2025).

42. Miles, A. J., Ramalli, S. G. & Wallace, B. A. DichroWeb, a website for calculating protein secondary structure from circular dichroism spectroscopic data. *Protein Science* **31**, 37–46 (2022).

43. Wang, J. *et al.* Elucidation of molecular interactions between selected phenylpropanoids and myofibrillar protein: Conformational remodeling and machine learning analysis. *Food Research International* **228**, 118268 (2026).

44. Ewald, J. D. *et al.* Web-based multi-omics integration using the Analyst software suite. *Nat Protoc* **19**, 1467–1497 (2024).

Figures

Fig.1 Changes in the conformation (A: total sulfhydryl content; B: free amine content; C: surface hydrophobicity) of MPs upon the addition of aldehydes during heat processing. Significant differences between the aroma compounds are indicated by different uppercase letters (A-E), while significant differences between the unheated (UH), heat up (HU), and cool down (CD) groups are indicated by different lowercase letters (a-c) ($P < 0.05$). (D)Stern–Volmer plots and (E)double logarithm plots were obtained at 298, 303, and 310 K.

Fig.2 SDS-PAGE patterns of MPs with the addition of different aldehydes. (A, D) unheated MPs with addition of aldehydes; (B, E) MPs after "heat up" with addition of aldehydes; (C, F) MPs after "cool down" with addition of aldehydes. Samples were prepared in the absence (-β) or presence (+β) of β-ME. Source data were shown in the Supplementary Information.

Fig.3 Changes in the microstructure of MPs under different treatment conditions. (A) particle size; (B) Atomic force microscopy images.

Fig.4 (A) Changes in the binding ability of MPs and aldehydes (HE, OC, NO, EE, DE, and UD) with different disrupting agents. The error bars represent the standard error, which was calculated from triplicate determinations. Different letters (a–d) indicated significant differences among disrupting agents ($P < 0.05$). (B) heatmap of flavor retention/release behavior. (C)The optimal binding models of aldehydes (HE, OC, NO, EE, DE, and UD) within the MPs binding pocket were depicted by molecular docking. Key interactions with specific amino acid residues are illustrated.

Fig.5 Machine learning cluster K-means analysis results.

Fig.6 Schematic modeling of the interactions of aldehydes-MPs.

Tables

Table 1 Secondary structure of MPs treated with aldehydes.

Table 2. Quenching constant (Kq), rate constant (Ksv), binding constant (Ka) and related thermodynamic parameters of different aldehydes-MPs interactions.

Table 3. Modified peptides identified by proteomics from MPs to which aldehydes were added.

Supplementary information

Fig.S1 The heating curve of SBS and MPs processing.

Fig.S2 MS/MS spectra of adduct peptides from HE, OC, NO, DD, DE, and UD.

Fig.S3 Source data of SDS-PAGE.

Table S1 Summary of studies on the interactions of flavor-protein.

Table S2 Physicochemical properties of aldehydes.

Table S3 Generalized estimating equations results for secondary structural changes by heat and aldehyde characteristics.

Table S4 Effect of various reagents on molecular interactions between proteins and flavor compounds.

Table S5 Binding sites and energies of MPs with aldehydes.

Table 1 Secondary structure of MPs treated with aldehydes.

Table 2. Quenching constant (Kq), rate constant (Ksv), binding constant (Ka) and related thermodynamic parameters of different aldehydes-MPs interactions.

Table 3. Modified peptides identified by proteomics from MPs to which aldehydes were added.

Table 1 Secondary structure of MPs treated with aldehydes.

Heat	Aldehydes	Total α-helix	Total β-sheets	Total β-turn	Total random coil
UH	HE	45.25 (45.22, 45.28)	10.93 (10.88, 10.94)	33.54 (33.52, 33.56)	10.32 (10.32, 10.33)
	OC	45.17 (45.17, 45.45)	10.91 (10.43, 11)	33.57 (33.56, 33.62)	10.4 (10.34, 10.58)
	NO	45.25 (31.37, 45.47)	9.94 (7.25, 10.44)	33.63 (33.57, 46.27)	10.64 (10.48, 14.85)
	DD	7.24 (6.67, 7.44)	68.98 (68.78, 69.65)	12.65 (12.58, 12.69)	11.09 (11.08, 11.11)
	DE	8.43 (8.38, 8.43)	67.1 (67.1, 67.14)	13.04 (13.04, 13.05)	11.45 (11.44, 11.49)
	UD	7.79 (7.34, 7.89)	68.22 (68.19, 68.94)	12.75 (12.6, 12.8)	11.12 (11.07, 11.18)
	CK	45.77 (45.59, 45.77)	9.96 (9.96, 10.24)	33.6 (33.59, 33.65)	10.66 (10.54, 10.66)
HU	HE	16.87 (16.16, 16.92)	38.04 (37.61, 39.51)	26.79 (26.36, 26.91)	18.4 (18.08, 18.57)
	OC	18.17 (17.01, 19.29)	37.12 (34.88, 38.53)	26.72 (26.4, 27.6)	18.14 (18.01, 18.31)
	NO	15.82 (15.77, 15.84)	39.94 (39.85, 39.97)	26.07 (26.07, 26.15)	18.21 (18.18, 18.21)
	DD	17.1 (16.54, 17.64)	37.75 (36.91, 38.57)	26.71 (26.49, 26.9)	18.44 (18.36, 18.51)
	DE	15.8 (15.52, 16.24)	39.92 (39.03, 40.54)	26.2 (26.01, 26.48)	18.19 (17.94, 18.31)
	UD	15.12 (14.99, 15.95)	41.49 (40.36, 41.79)	25.84 (25.81, 26.02)	17.51 (17.42, 17.66)
	CK	15.09 (14.5, 15.24)	41.61 (40.98, 43.16)	25.82 (25.4, 25.96)	17.58 (17, 17.83)
CD	HE	18.3 (17.5, 18.77)	37.11 (36.25, 37.59)	26.81 (26.8, 27.02)	18.25 (18.08, 18.38)
	OC	16.96 (16.77, 18.1)	37.86 (36.58, 37.93)	26.86 (26.78, 27.04)	18.4 (18.23, 18.49)
	NO	17.55 (17.32, 17.9)	36.91 (36.56, 37.36)	27.22 (27.19, 27.28)	18.15 (18.1, 18.19)
	DD	18.69 (18.31, 19.59)	34.8 (33.35, 35.77)	27.62 (27.33, 28.2)	18.79 (18.56, 18.81)
	DE	6.93 (6.75, 7.02)	70.01 (69.82, 70.34)	12.31 (12.19, 12.39)	10.75 (10.68, 10.78)
	UD	7.66 (7.29, 8.33)	68.85 (67.64, 69.45)	12.46 (12.38, 12.83)	11.03 (10.89, 11.21)
	CK	15.78 (15.74, 17.4)	39.9 (37.79, 40)	26.1 (26.07, 26.65)	18.2 (18.2, 18.22)
wald X^2		wald X^2_{heat}= 147.3 wald $X^2_{aldehyde}$=5976.90	wald X^2_{heat}=777.70 wald $X^2_{aldehyde}$=8511.84	wald X^2_{heat}=605.33 wald $X^2_{aldehyde}$=15218.77	wald X^2_{heat}=698.87 wald $X^2_{aldehyde}$=1897.07
P		$P_{heat} < 0.001$ $P_{aldehyde} < 0.001$	$P_{heat} < 0.001$ $P_{aldehyde} < 0.001$	$P_{heat} < 0.001$ $P_{aldehyde} < 0.001$	$P_{heat} < 0.001$ $P_{aldehyde} < 0.001$

Note: Data represented as P50(P25, P75) of three independent experiments.

Table 2. Quenching constant (Kq), rate constant (Ksv), binding constant (Ka) and related thermodynamic parameters of different aldehydes-MPs interactions.

ACs	T(K)	Stern-Volmer quenching constants			Binding parameters			Thermodynamic parameters		
		Ksv (10^3L·mol^{-1})	Kq (10^{11}L·mol^{-1}·s^{-1})	R_1^2	Ka (10^3L·mol^{-1})	n(-)	R_2^2	ΔG (kJ·mol^{-1})	ΔH（kJ·mol^{-1}）	ΔS（kJ·mol^{-1}·K^{-1}）
HE	298	35.31	35.31	0.9289	31.00	1.95	0.98	-25.62	-80.57	-0.19
	303	16.55	16.55	0.9306	14.56	1.65	0.9471	-24.15		
	310	8.81	8.81	0.9393	8.62	3.08	0.9142	-23.36		
OC	298	8.91	8.91	0.9116	8.21	1.09	0.9417	-22.33	9.77	0.11
	303	5.68	5.68	0.9262	5.33	1.40	0.979	-21.62		
	310	9.29	9.29	0.9773	9.13	1.38	0.9798	-23.50		
NO	298	0.56	0.56	0.955	1.42	1.01	0.9808	-17.98	6.62	0.08
	303	2.03	2.03	0.9071	1.73	1.04	0.9266	-18.79		
	310	1.09	1.09	0.9706	1.59	0.72	0.9522	-19.00		
DD	298	4.77	4.77	0.971	4.57	0.87	0.903	-20.88	4.76	0.09
	303	3.55	3.55	0.9783	3.77	0.84	0.9618	-20.75		
	310	4.14	4.14	0.9499	4.82	0.70	0.9432	-21.86		
DE	298	3.23	3.23	0.969	3.14	0.91	0.9337	-19.95	49.26	0.23
	303	2.34	2.34	0.9562	2.58	0.99	0.9281	-19.79		
	310	6.17	6.17	0.9178	6.46	1.36	0.9211	-22.61		
UD	298	7.55	7.55	0.909	6.79	2.19	0.9773	-21.86	35.03	0.19
	303	13.54	13.54	0.9428	12.03	2.31	0.9761	-23.67		
	310	14.20	14.20	0.9433	12.11	1.88	0.9859	-24.23		

Table 3. Modified peptides identified by proteomics from MPs to which aldehydes were added.

Aroma compound	Modified peptide	Type of reaction	Protein name	Molecular weight (Da)	q-value
HE	MK(+82.08 Da)EEEVEALMAGQEDSNGCINYEAFVK	Schiff base	Myosin light chain 1/3, skeletal muscle isoform	3148.4159	0.0079
	DLEEATLQHEAMVAALR(+82.08 Da)	Schiff base	MYH3 protein	1995.0215	0.003
OC	NTK(+110.11 Da)YSVMINGPSYPR	Schiff base	Troponin C	1852.9625	0.006
NO	DPMR(+124.13 Da)AIVPILLDANVSTYDK(+124.13 Da)	Schiff base	Myosin heavy chain	2479.4242	0.064
DD	ALGTNPTNAEVK(+134.11 Da)K(+134.11Da)	Schiff base	Myosin light chain 1/3, skeletal muscle isoform	1610.9515	0.003
	LMAGQEDSNGC(+152.12 Da)INYEAFVK	Michael addition	Myosin light chain 3	2241.0566	0.003
	KFLEELLTTQC(+152.12 Da)DR	Michael addition	Myosin regulatory light chain 2, skeletal muscle isoform	1747.9299	0.003
	SFLVW(+152.12 Da)VNEEDHLR	Michael addition	Creatine kinase M-type	1795.9377	0.003
	TLEDQMNEH(+152.12 Da)R	Michael addition	Myosin heavy chain 7	1424.6838	0.003
	MDIAIHH(+152.12 Da)PWIR	Michael addition	Alpha-crystallin B chain	1582.8563	0.003
	NIC(+152.12 Da)YVITHGDAK	Michael addition	Myosin regulatory light chain 2, skeletal muscle isoform	1485.7770	0.003
	NIC(+152.12 Da)YVITHGDAKDQE	Michael addition	Myosin regulatory light chain 2, skeletal muscle isoform	1857.9051	0.003
	AVNDLGTVEIEC(+152.12 Da)K	Michael addition	MYBPC1 protein	1542.8084	0.003
	AVNELGEALAEC(+152.12 Da)K	Michael addition	Myosin binding protein C2	1498.7821	0.003
	C(+152.12 Da)SELEEELK	Michael addition	Tropomyosin alpha-3 chain	1231.6126	0.003

	IQFSQC(+152.12 Da)GDVMR	Michael addition	Myosin light chain 6B	1435.7072	0.0007
	H(+152.12 Da)KVCMDLR	Michael addition	Troponin I2, fast skeletal type	1153.6220	0.0007
	C(+152.12 Da)QLPEDVDPTSVTSALR	Michael addition	Heat shock protein family B (small) member 7	1983.0103	0.0013
	EC(+152.12 Da)WEQEHEER	Michael addition	Troponin I1, slow skeletal type	1526.6580	0.0021
	H(+152.12 Da)IAEDSDR	Michael addition	Tropomyosin beta chain	1094.5477	0.0021
	EICLK(+152.12 Da)CEVSENITGK	Michael addition	MYBPC1 protein	1817.9387	0.0071
DE	FEVSFGR(+154.14 Da)EGETMSLGCSVVITPEIK	Michael addition	Myomesin 1	2926.4941	0.0010
UD	LMK(+168.15 Da)DNFPNFLGACEK(+168.15 Da)	Michael addition	Myosin light chain 6	2120.1534	0.0071

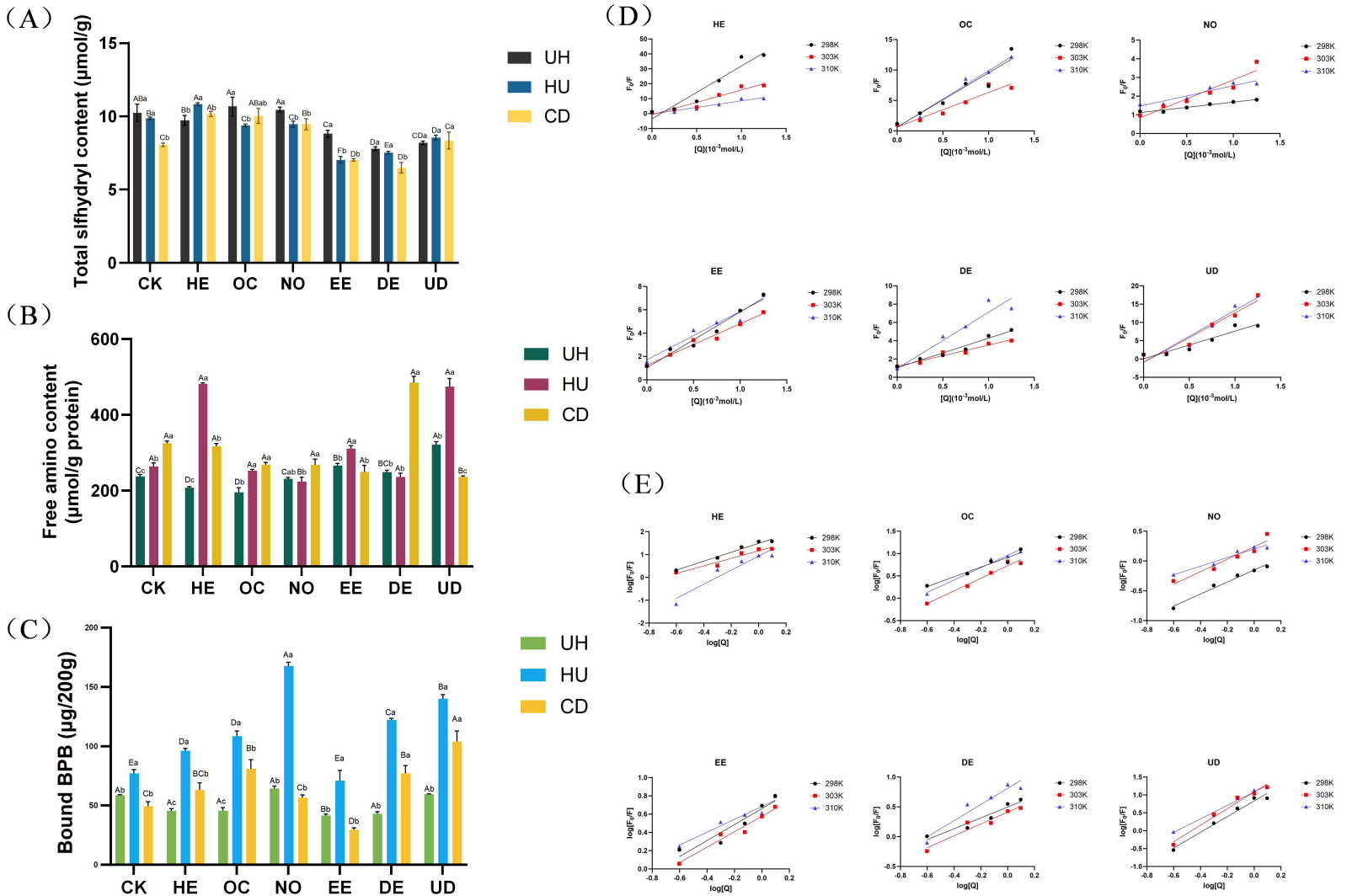
(A)
Total slfhydryl content (μmol/g)
UH
HU
CD
CK HE OC NO EE DE UD
(B)
Free amino content (μmol/g protein)
UH
HU
CD
CK HE OC NO EE DE UD
(C)
Bound BPB (μg/200g)
UH
HU
CD
CK HE OC NO EE DE UD
(D)
HE
OC
NO
EE
DE
UD
298K
303K
310K
[Q](10-3mol/L)
(E)
HE
OC
NO
EE
DE
UD
298K
303K
310K
log[Q]

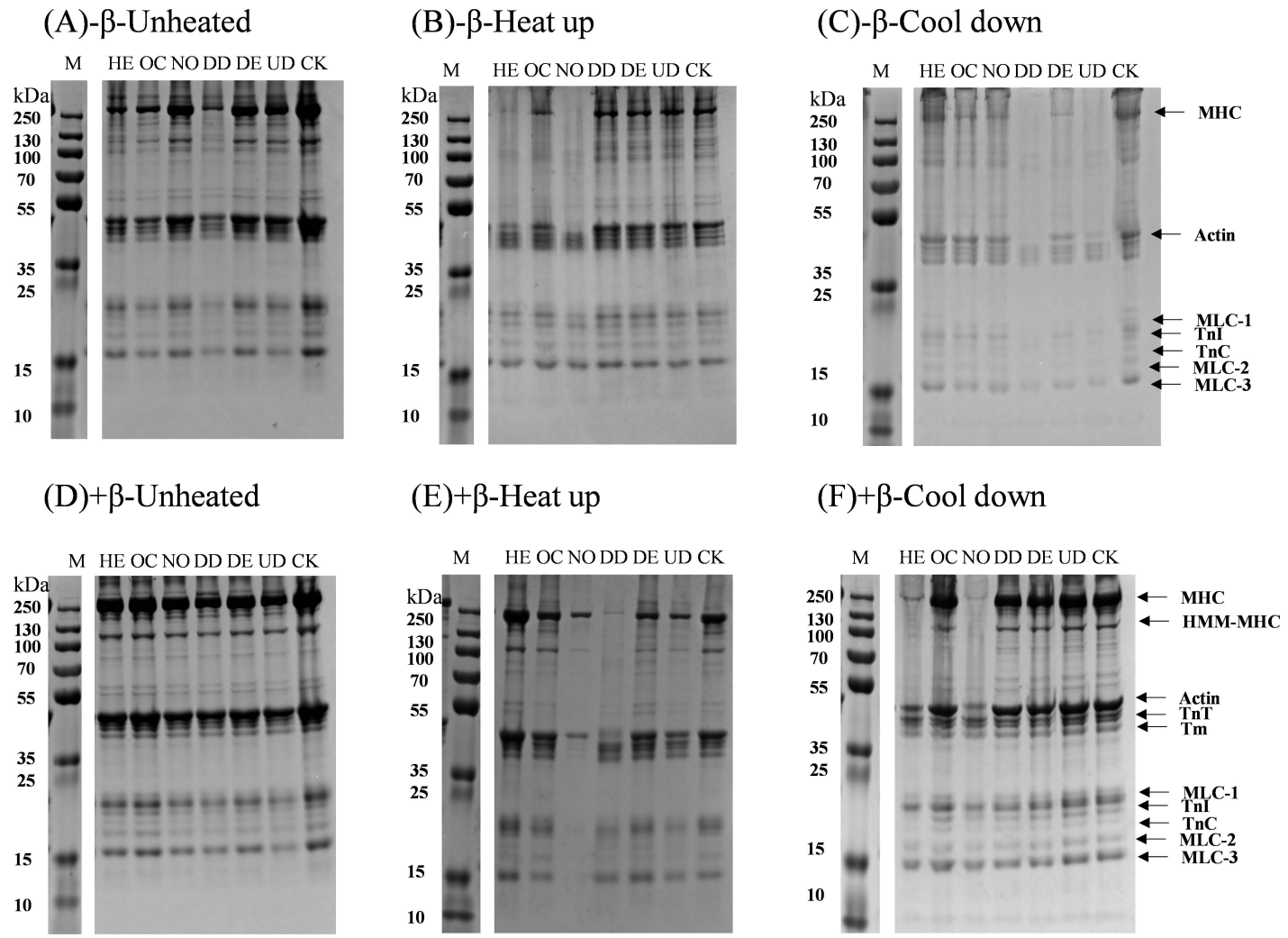

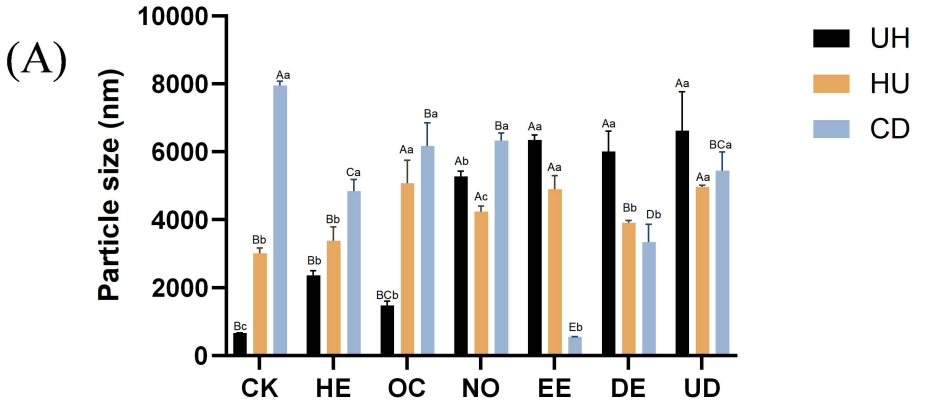
(A)
Particle size (nm)
10000
8000
6000
4000
2000
0
UH
HU
CD
Bc
Bb
Aa
Bb
Bb
Ca
BCb
Aa
Ba
Ab
Ac
Ba
Aa
Aa
Eb
Aa
Bb
Db
Aa
Aa
BCa
CK
HE
OC
NO
EE
DE
UD

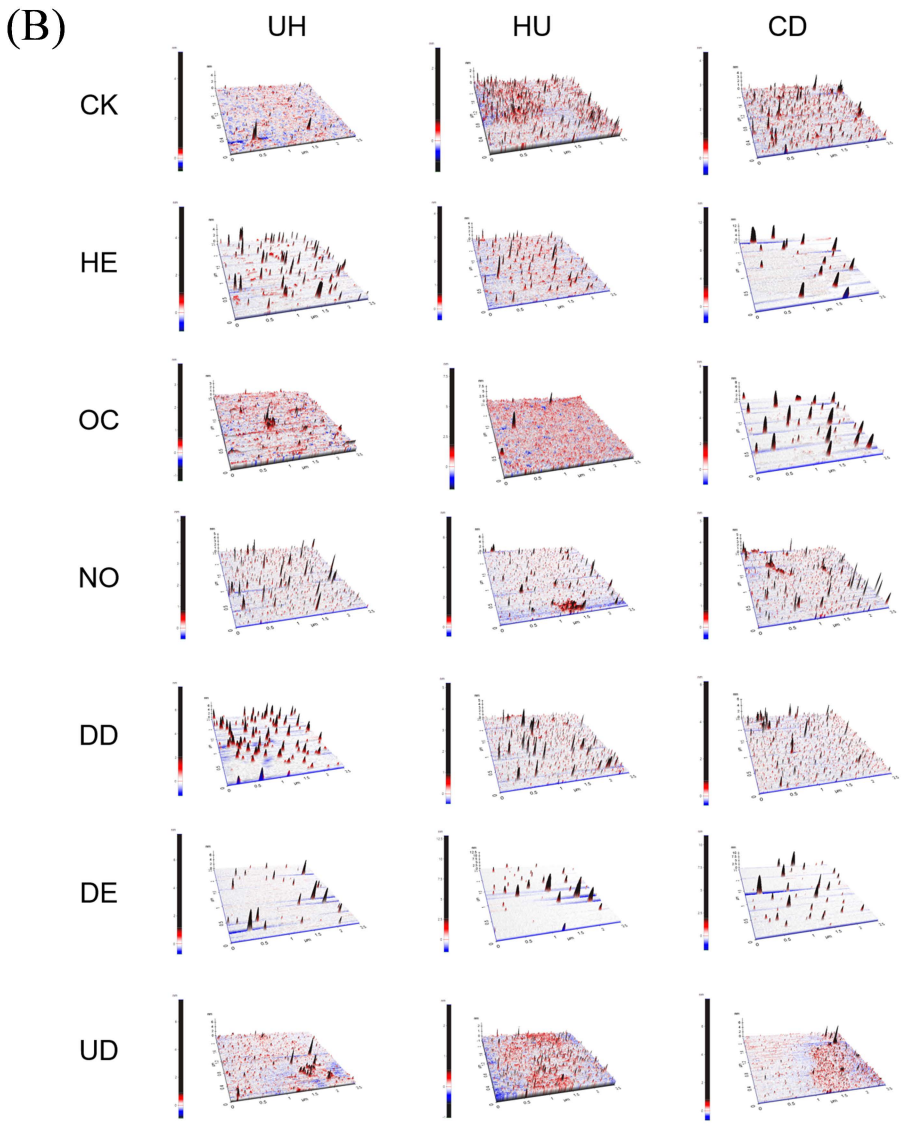
(B)
UH
HU
CD
CK
HE
OC
NO
DD
DE
UD

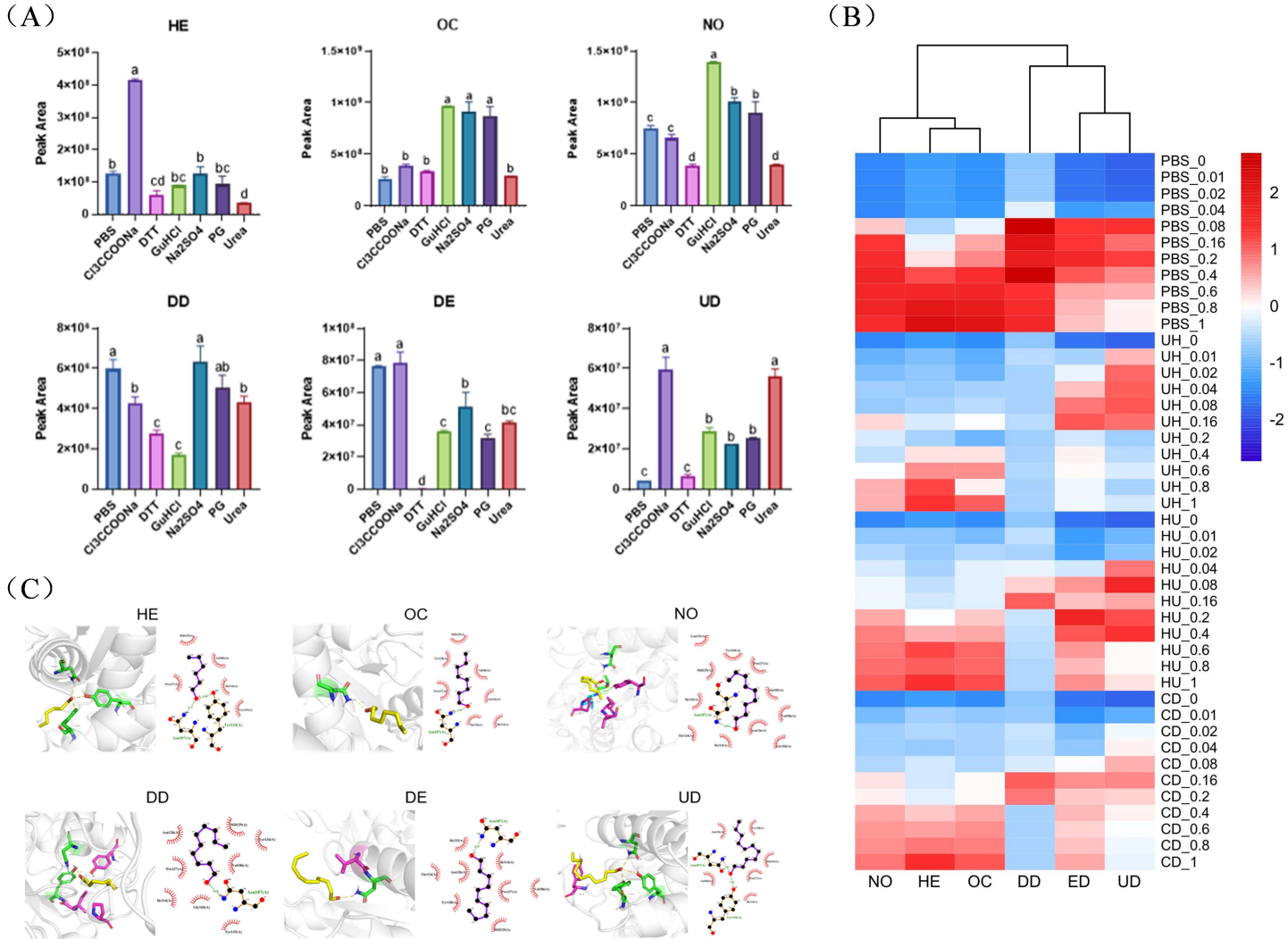
(A)
HE
OC
NO
DD
DE
UD
Peak Area
PBS
Cl3CCOONa
DTT
GuHCl
Na2SO4
PG
Urea
(B)
PBS_0
PBS_0.01
PBS_0.02
PBS_0.04
PBS_0.08
PBS_0.16
PBS_0.2
PBS_0.4
PBS_0.6
PBS_0.8
PBS_1
UH_0
UH_0.01
UH_0.02
UH_0.04
UH_0.08
UH_0.16
UH_0.2
UH_0.4
UH_0.6
UH_0.8
UH_1
HU_0
HU_0.01
HU_0.02
HU_0.04
HU_0.08
HU_0.16
HU_0.2
HU_0.4
HU_0.6
HU_0.8
HU_1
CD_0
CD_0.01
CD_0.02
CD_0.04
CD_0.08
CD_0.16
CD_0.2
CD_0.4
CD_0.6
CD_0.8
CD_1
NO
HE
OC
DD
ED
UD
(C)
HE
OC
NO
DD
DE
UD

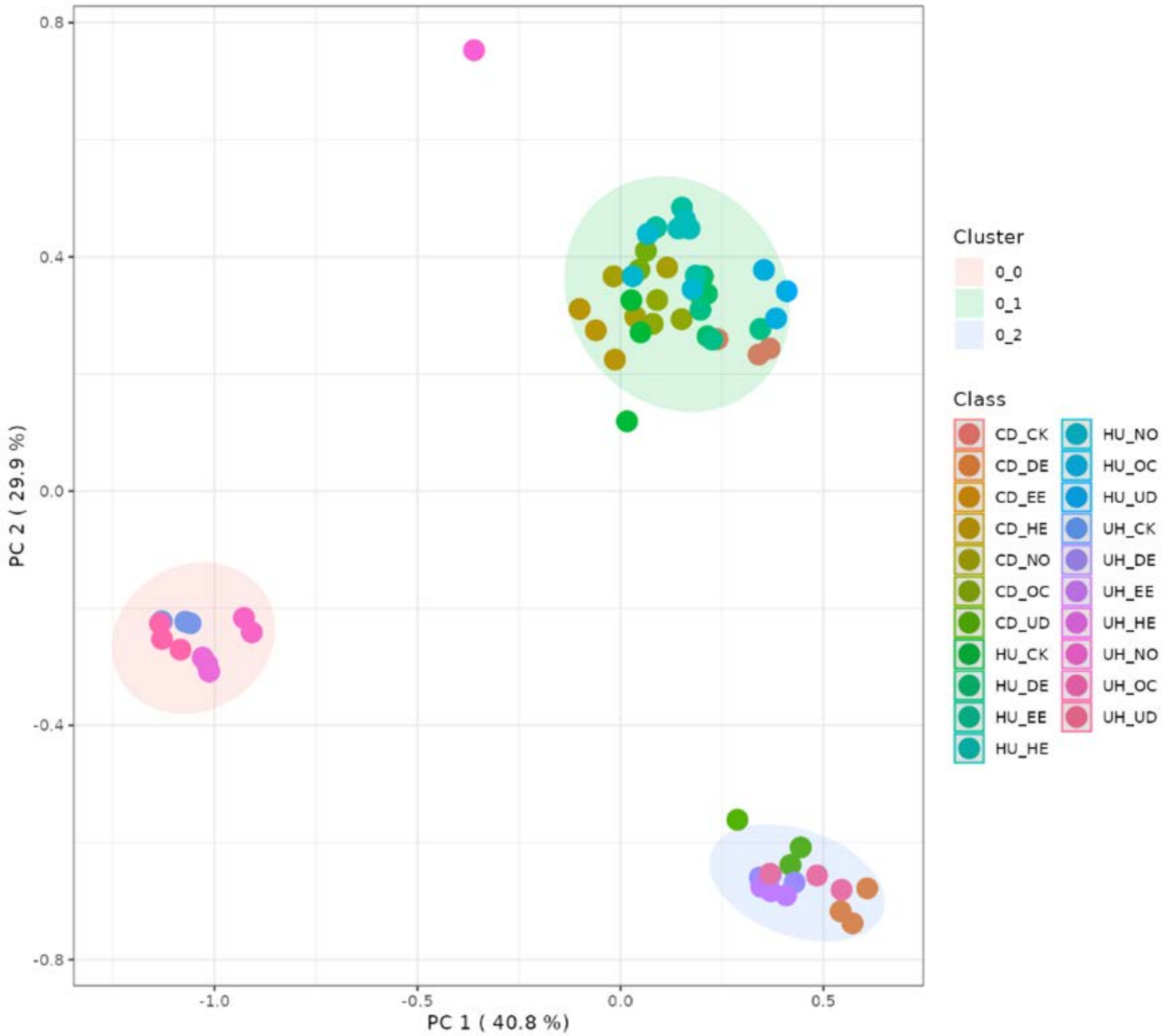

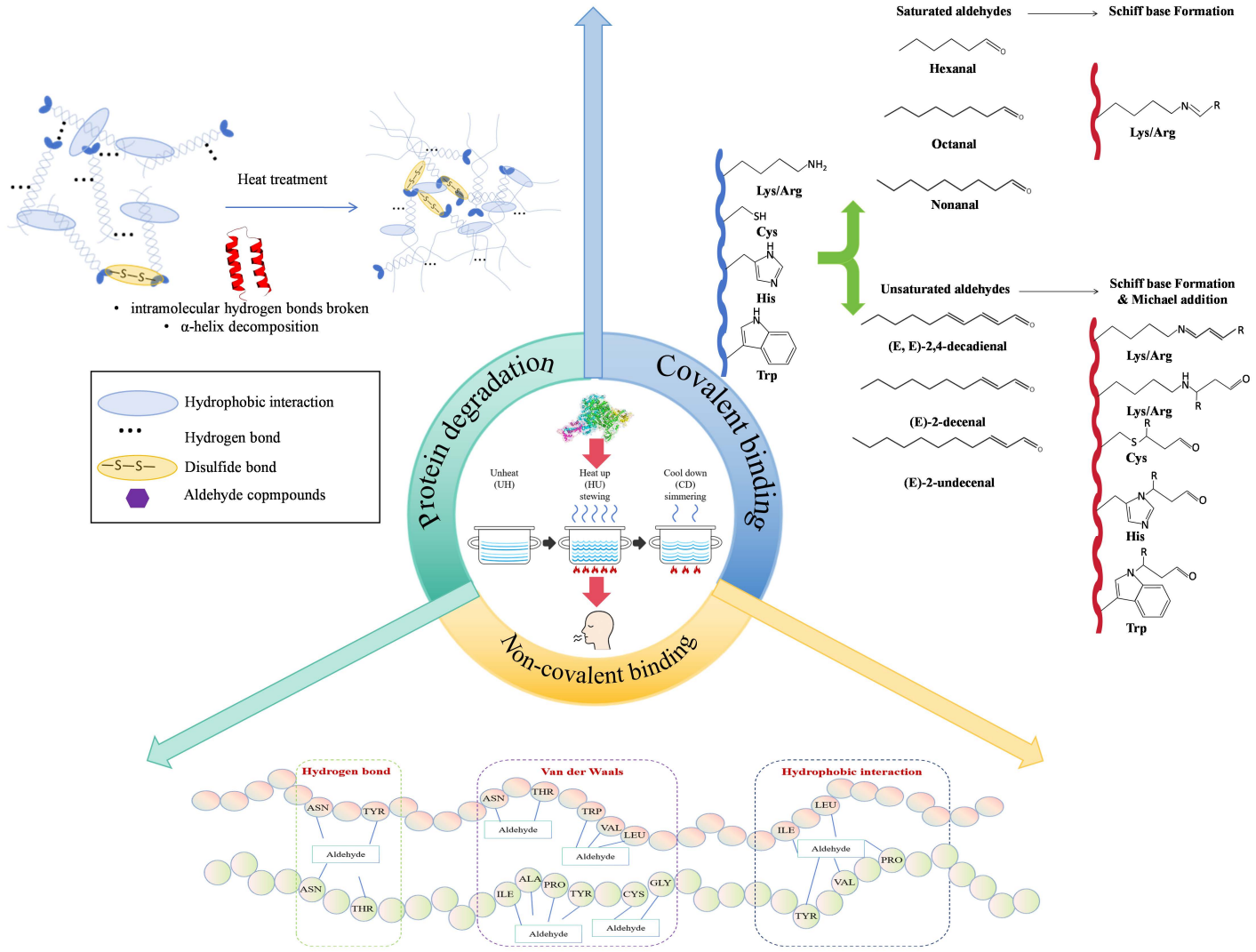
Heat treatment
• intramolecular hydrogen bonds broken
• α-helix decomposition
Hydrophobic interaction
Hydrogen bond
Disulfide bond
Aldehyde copmpounds
Protein degradation
Covalent binding
Non-covalent binding
Unheat (UH)
Heat up (HU) stewing
Cool down (CD) simmering
Saturated aldehydes
Schiff base Formation
Hexanal
Octanal
Nonanal
Lys/Arg
Unsaturated aldehydes
Schiff base Formation & Michael addition
(E, E)-2,4-decadienal
(E)-2-decenal
(E)-2-undecenal
Lys/Arg
Cys
His
Trp
Hydrogen bond
Van der Waals
Hydrophobic interaction
Aldehyde
ASN
TYR
THR
TRP
VAL
LEU
ALA
PRO
ILE
CYS
GLY